Observation of Electron Diffraction and Determination of Lattice Spacing in Graphite

Peter Khorani

PHY 353L Modern Laboratory
Department of Physics
The University of Texas at Austin
Austin, TX 78712, USA

October 28, 2025

Abstract

In this experiment, we investigate the de Broglie wavelength of accelerated electrons using a Teltron model 555 electron–diffraction tube driven by a model 813 power unit (up to 5 kV). Electrons are emitted, accelerated through a potential V, and pass through a thin polycrystalline graphite target. The resulting diffraction pattern on a phosphor screen consists of concentric rings arising from interplanar spacings of 2.13 Å and 1.23 Å. We photographed the pattern for accelerating voltages from 2.00 to 5.00 kV in 0.25 kV steps using a fixed camera distance of 0.456 m (for image scaling). A custom Python routine measured ring radii and computed λ via $\lambda = d\,r/L$. The extracted wavelengths agree with the de Broglie prediction $\lambda_{\mathrm{th}} = h/\sqrt{2meV}$ across the full range with relative deviations below ≈0.25%. Independent string-and-marker measurements (using the tube's internal foil–screen distance $L_{\mathrm{tube}} = 125(2)$ mm) yielded ring diameters consistent with theory to within $\sim 5\%$. These results confirm the wave nature of electrons and illustrate the effectiveness of automated image processing for precision undergraduate measurements.

1 Introduction

1.1 Motivation

Wave–particle duality is a cornerstone of quantum mechanics: matter exhibits wave-like behavior characterized by the de Broglie relation $\lambda = h/p$. A direct, quantitative demonstration is provided by electron diffraction from crystalline solids. When a narrow electron beam traverses a thin polycrystalline graphite foil, constructive interference from lattice planes produces a set of concentric rings on a fluorescent screen. Measuring the ring geometry as a function of accelerating voltage V tests both the de Broglie hypothesis and Bragg's law in a single, table-top experiment suitable for an advanced instructional laboratory.

Beyond its pedagogical value, electron diffraction underpins modern optical methods such as transmission electron microscopy (TEM) and low-energy electron diffraction (LEED), where crystal structure, lattice spacings, and orientation are inferred from diffraction features. The Teltron electron-diffraction tube provides an accessible analogue: a thermionic electron gun accelerates electrons through a controllable potential and directs them through a thin graphite target with well-known interplanar spacings, producing bright, easily photographed rings. By analyzing how ring diameters scale with V, one can extract $\lambda(V) \propto V^{-1/2}$ and verify quantitative agreement with theory.

In this study, I pursued two goals. First, we measured ring diameters across $V = 2.00$ to $5.00\,\mathrm{kV}$ in $0.25\,\mathrm{kV}$ increments and compare the inferred wavelengths to $\lambda_{\mathrm{th}} = h/\sqrt{2meV}$ (with relativistic correction). Second, I compared two ways of measurements – (i) manual diameters obtained with a string and calipers on the bulb, using the tube's internal camera length L_{tube}, and (ii) automated image processing of photographs using a fixed camera distance for pixel–to–mm scaling. This dual approach lets us assess systematic effects (centering, parallax, scale calibration) and quantify the accuracy and precision achievable with each method. The resulting analysis provides a clear, quantitative confirmation of electron wave behavior and a practical demonstration of uncertainty-aware data processing in a modern lab setting.

1.2 Theoretical background

de Broglie wavelength. Matter waves associate a wavelength λ with particle momentum p via de Broglie's relation

$$\lambda = \frac{h}{p}. \tag{1}$$

For electrons accelerated through a potential V, the non-relativistic kinetic energy is $K = eV = p^2/(2m_e)$, giving

$$\lambda_{\mathrm{nr}} = \frac{h}{\sqrt{2m_e eV}}. \tag{2}$$

At a few kilovolts, the relativistic correction is small but non-negligible; incorporating it yields

$$\lambda(V) \;=\; \frac{h}{\sqrt{2m_e eV\left(1+\frac{eV}{2m_e c^2}\right)}}, \tag{3}$$

so that $\lambda \propto V^{-1/2}$ to leading order.[2]

Bragg condition for a polycrystalline foil. Diffraction from planes with spacing d satisfies Bragg's law

$$2d\,\sin\theta = n\,\lambda, \tag{4}$$

with scattering half-angle θ and integer order n.[3] In a *polycrystalline* foil, randomly oriented crystallites produce a cone of diffracted intensity for each allowed (hkl) family; the fluorescent screen intercepts these cones as concentric rings. For the Teltron graphite target the dominant spacings are approximately

$$d_1 \approx 0.213\,\mathrm{nm} \quad \text{and} \quad d_2 \approx 0.123\,\mathrm{nm},$$

which generate the inner and outer rings, respectively (cf. apparatus notes).

Screen geometry and ring diameter. Let L be the (internal) camera length, i.e. the separation from the foil plane to the screen along the beam axis. The ring radius r on the screen is related to the scattering angle by simple geometry:

$$\tan(2\theta) = \frac{r}{L}. \tag{5}$$

For small angles (valid here), $\tan(2\theta) \approx 2\theta$, and combining (4)–(5) gives

$$r \approx \frac{L}{d}\lambda \quad \Longrightarrow \quad D \equiv 2r \approx \frac{2L}{d}\lambda. \tag{6}$$

Thus each ring's diameter scales inversely with the corresponding plane spacing d, and directly with λ and L. Ring *ratios* eliminate L: for two spacings d_1, d_2 at fixed V,

$$\frac{D_1}{D_2} \approx \frac{d_2}{d_1}. \tag{7}$$

Validity of approximations: For the largest rings (2 kV, outer) the small-angle error in $\tan(2\theta) \approx 2\theta$ is $\sim 1.4\%$, falling to $\sim 0.6\%$ at 5 kV. The relativistic wavelength is smaller than the nonrelativistic value by 0.10% (2 kV) to 0.24% (5 kV).

Voltage dependence. Using (3) in (6) at fixed L and d,

$$D(V) \propto \lambda(V) \propto \frac{1}{\sqrt{V}} \quad \text{(with small relativistic corrections).} \tag{8}$$

Consequently, plots of D (or r) versus $1/\sqrt{V}$ should be linear, and separately, D_1/D_2 should be constant and equal to d_2/d_1. These two checks—*voltage scaling* and *ring-ratio constancy*—are central consistency tests we will apply to our data in Sec. 3.

Notation and assumptions. We take V to be the accelerating potential applied to the electron gun anode, L the internal camera length (foil–to–screen distance inside the tube), d an interplanar spacing of graphite, θ the Bragg half–angle, λ the electron de Broglie wavelength, r the ring radius on the screen, and $D = 2r$ the ring diameter. Throughout the analysis we assume: (i) first–order diffraction ($n = 1$), (ii) small angles so that $\tan(2\theta) \approx 2\theta$, (iii) an isotropic polycrystalline target that produces circular cones of diffracted intensity, (iv) negligible multiple scattering and refraction in the thin foil, and (v) a relativistically corrected electron wavelength $\lambda(V)$ as in Eq. (3). For instrument parameters we use $L_{\text{tube}} = 125(2)\,\text{mm}$ from the apparatus notes for comparisons made directly on the bulb, while the external camera distance (0.456 m) is used only to set a consistent pixel–to–mm scale in photographs. Reported uncertainties include the voltmeter resolution ($\pm 0.01\,\text{kV}$), manual diameter readout ($\pm 0.02\,\text{mm}$ caliper precision plus centering/parallax), and image–analysis contributions (pixel scale, center refinement, ring–peak selection).

1.3 Our approach

We pursued two ways of measurement across $V = 2.00$ to $5.00\,\mathrm{kV}$ in $0.25\,\mathrm{kV}$ increments:

(1) Manual diameters on the bulb. For each voltage, we traced inner and outer ring diameters on the glass envelope using a string and marker, then read the chord length with calipers. Using the tube's internal camera length L_{tube} and Eq. (6), we converted D to λ and compared it with $\lambda(V)$ from Eq. (3). This channel is sensitive to centering and parallax, which we will include in the uncertainty discussion.

(2) Automated image analysis. We photographed each pattern at a fixed external camera distance (for a constant pixel scale) and processed the images with a Python workflow that (i) normalizes exposure, (ii) refines the beam center by maximizing ring circularity, (iii) forms an azimuthal radial profile, (iv) suppresses the central hot spot and the phosphor edge by restricting the search window, and (v) detects ring peaks (with optional manual confirmation). A ruler visible in the $2.00\,\mathrm{kV}$ frame supplies a fixed pixel–to–mm scale that is reused across images; resolution changes (e.g., HEIC $\rightarrow$ JPEG or sensor mode changes) are compensated by scaling with image width. From the measured radii $r(V)$ we compute $D(V)$, infer $\lambda(V) = d\,D/(2L_{\mathrm{tube}})$, and test the expected $D \propto V^{-1/2}$ scaling.

Consistency checks and fits. We perform two key internal checks: (i) ring–ratio constancy $D_1/D_2 \approx d_2/d_1$ at fixed V, and (ii) linearity of D (or r) versus $1/\sqrt{V}$. We also invert Eq. (6) to fit an effective L from the data, $L_{\mathrm{fit}} = D\,d/(2\lambda)$, as a cross–validation of the apparatus geometry. A full uncertainty analysis (propagation from V, L_{tube}, centering, pixel scale, and peak selection) accompanies the results in Sec. 3.

2 Experimental setup

2.1 Apparatus

The experiment employs a Teltron electron–diffraction tube (model 555) driven by a Teltron high-voltage power unit (model 813). The tube contains an indirectly heated oxide-coated cathode, control grid, and an anode that accelerates a narrow electron beam through a thin polycrystalline graphite target mounted on a fine mesh. Diffracted electrons form concentric rings on a phosphor screen integral to the glass envelope. The dominant graphite spacings are $d_1 \approx 0.213\,\mathrm{nm}$ and $d_2 \approx 0.123\,\mathrm{nm}$, which yield the inner and outer rings, respectively (see manufacturer documentation).[1]

The power unit provides a continuously adjustable accelerating potential in the range used here, 2.00 to 5.00 kV in 0.25 kV steps, with an instrument resolution of ±0.01 kV. The effective internal camera length, a.k.a. the separation between the graphite foil plane and the screen along the beam axis—was taken as

$$L_{\text{tube}} = 125(2)\,\text{mm},$$

which is different from the path length shown in Figure 1, however it will be used for all physics conversions between ring diameter and wavelength via Eq. (6).

For photographic acquisition, the tube was mounted on an optical bench, and images of the screen were recorded with a fixed external camera distance of 0.456 m (lens to bulb front). A millimeter ruler was positioned in the 2.00 kV frame to supply a pixel-to-mm scale that is reused across all images (resolution changes are compensated as described in Sec. 3). The camera distance is used solely for image scaling; it does not enter the diffraction geometry.

Table 1: Key apparatus parameters. Uncertainties are one standard deviation unless noted.

Quantity	**Symbol**	**Value**
Accelerating voltage range	V	2.00 to 5.00 kV (step 0.25 kV)
Voltage readout resolution		±0.01 kV
Foil–to–screen distance (camera length)	L_{tube}	125(2) mm
Dominant graphite spacings	d_1, d_2	0.213 nm, 0.123 nm
Screen type		Phosphor (integral to tube)
External camera distance (for scaling)		0.456 m
Manual diameter readout		String trace + calipers (±0.02 mm resolution)

2.2 Data Collection

Voltage sweep. We acquired diffraction patterns for accelerating voltages $V = 2.00\,\text{kV}, 2.25\,\text{kV}, \ldots, 5.00\,\text{kV}$ in $\Delta V = 0.25\,\text{kV}$ increments (13 images/measurements total). The power-unit readout resolution was ±0.01 kV. At each setting we waited several seconds for beam and brightness to stabilize before recording measurements.

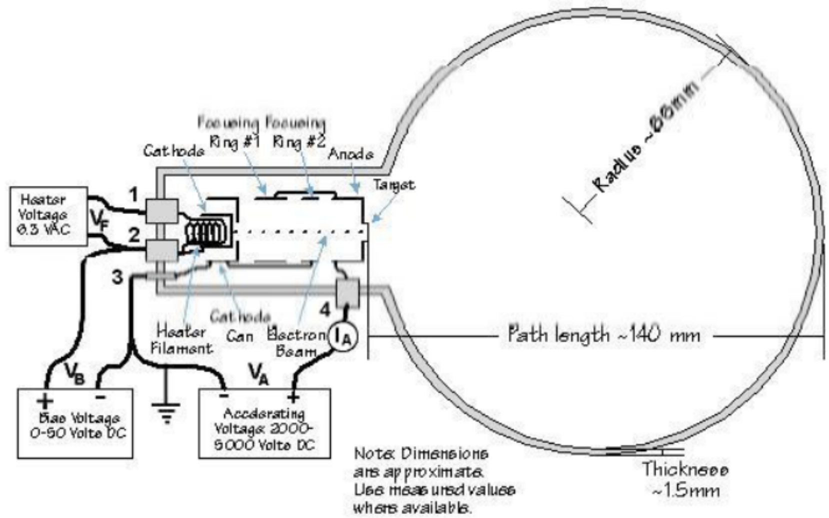

Figure 1: Schematic of the Teltron electron–diffraction tube and geometry: electrons are accelerated through V_A, pass a polycrystalline graphite foil at the tube center (the Target), and produce rings on the phosphor screen a distance L_{tube} downstream. (This was taken from the Lab Manual)

Manual diameters on the bulb. For every V the inner and outer rings were traced directly on the glass using a taut string passed across the apparent center; the chord length was then read with calipers ($\pm 0.02\,\text{mm}$ resolution). The diameter uncertainties are dominated by centering and parallax on the curved envelope; we estimate an additional placement uncertainty of $\mathcal{O}(\pm 0.5\,\text{mm})$ that is propagated in Sec. 3. These diameters are converted to wavelengths using Eq. (6) with the internal camera length $L_{\text{tube}} = 125(2)\,\text{mm}$.

Photographic acquisition. The tube was mounted on an optical bench and photographed at a fixed external camera distance of $0.456\,\text{m}$ (lens to bulb front). A millimeter ruler was positioned adjacent to the screen in the $2.00\,\text{kV}$ frame to set the pixel-to-mm scale; the same scale is reused for all subsequent images. To accommodate occasional changes in sensor mode/HEIC-to-JPEG conversion (e.g., 4032×3024 to 5712×4284 at $2.75\,\text{kV}$), I rescaled the pixel size by the image width ratio so that the physical mm scale is consistent across the dataset. Room lights were dimmed for contrast, and exposure was adjusted to avoid saturation at the center spot.

3 Data Analysis and Results

3.1 Data Processing and Hypothesis Testing

Image-analysis workflow (implementation order). The processing follows the exact sequence implemented in my Python code.

1. **Calibration and scaling.** If a calibration file is not provided, the user clicks two endpoints of a known span on the ruler; pixels-per-mm is stored together with the calibration image size. When processing any image, the pixel scale is adjusted by the width ratio $w_{\text{cur}}/w_{\text{calib}}$ so that mm units remain consistent across different sensor modes/resolutions.

2. **Read and prefilter.** The image is converted to grayscale, normalized to $[0, 1]$, and median–filtered (radius 1) to suppress salt-and-pepper noise.

3. **Initial center estimate.** A brightness–squared centroid is computed on the right 65% of the frame (to avoid the ruler), yielding $(c_x^{(0)}, c_y^{(0)})$.

4. **Radial profile (seed).** An azimuthal average $I(r)$ is formed about $(c_x^{(0)}, c_y^{(0)})$ over many angles; an optional angular wedge $[\theta_0, \theta_1]$ can be masked to ignore glare or the ruler. The profile is smoothed with a moving average ($k = 11$).

5. **Center refinement (optional).**

   (a) Auto: A seed ring radius is taken from the strongest peak in the smoothed profile (fallback: the maximum in the first third of samples). The center is refined by searching an integer grid ± 5 px around $(c_x^{(0)}, c_y^{(0)})$ and choosing the point that minimizes the standard deviation of ring radii measured as a function of angle (i.e., maximizes circularity).

   (b) Manual: The user clicks the center once. – I actually preferred this one.

   A new profile $I(r)$ is computed about the final center and smoothed again.

6. **Peak selection.**

(a) Auto: Local maxima are found with a minimum separation of 20 px and a relative threshold of 0.05; the two smallest-radius peaks are taken as inner/outer rings.

(b) Manual: The user clicks peak locations on $I(r)$; clicks are snapped to the nearest profile samples. – Once again, I preferred this one. The code wasn't too good at identifying specific peak locations, especially if they were small bumps.

7. **Unit conversion and optional physics.** Radii in pixels are converted to mm via the (possibly rescaled) pixel size; diameters $D = 2r$ are reported. If a tube camera length L is supplied and the accelerating voltage V is parsed from the filename (regex), the relativistic electron wavelength $\lambda(V)$ and per-ring d values are computed.

8. **Outputs.** For each image the script saves a profile plot (raw + smoothed with peak markers) and appends a row to `measurements_v2.csv` containing the center, radii, diameters, pixel scale, and (if available) λ and d.

Uncertainty model. Diameter uncertainty combines (i) caliper resolution on the string trace, (ii) center placement and parallax on the bulb (manual channel), and (iii) pixel scale and center-refinement error (image channel). We treat these as independent:

$$\sigma_D^2 \;=\; \sigma_{\text{read}}^2 + \sigma_{\text{center}}^2 + \sigma_{\text{scale}}^2. \tag{9}$$

Wavelength is obtained from $\lambda = d\,D/(2L)$, so

$$\left(\frac{\sigma_\lambda}{\lambda}\right)^2 \;=\; \left(\frac{\sigma_D}{D}\right)^2 + \left(\frac{\sigma_L}{L}\right)^2 \quad \text{(with } d \text{ taken from the graphite target).} \tag{10}$$

For voltage-dependent checks we use the relativistic $\lambda(V)$; its uncertainty from the voltmeter (± 0.01 kV) is $< 0.1\%$ and is negligible compared to geometric terms.

Replicates and consistency. At several voltages we recorded multiple images to assess repeatability. Consistency checks included: (i) linearity of D vs. $1/\sqrt{V}$, (ii) constancy of the ratio $D_{\text{inner}}/D_{\text{outer}} \approx d_2/d_1$, and (iii) an effective-length back-fit $L_{\text{fit}} = D\,d/(2\lambda)$ compared to L_{tube}. Discrepant frames (e.g., with motion blur or clipped highlights) were excluded prior to analysis.

Mode choice and calibration transfer. Although both auto and manual options were implemented, the final radii used for fitting were selected in **manual** mode for all voltages because weak bumps in $I(r)$ occasionally fooled the auto peak finder. The 2.00 kV ruler set the reference pixel scale (pixels per mm). For images with different sensor resolutions or HEIC→JPEG conversions, the scale was transferred by the width ratio $s = w_{\rm cur}/w_{\rm calib}$, i.e. mm per $\text{px}_{\rm cur}$ = mm per $\text{px}_{\rm calib}/s$. So the calibration size for the 5712 x 4284 (24 MP) images was upscaled by 1.416× the original amount from the 4032 x 3024 (12 MP) image that had the original calibration.

Consistency tests and fits. At fixed V, the ring ratio $R \equiv D_1/D_2$ should equal d_2/d_1 (Sec. 1.2). We report $R(V)$ with uncertainty $\sigma_R \approx R\sqrt{(\sigma_{D_1}/D_1)^2 + (\sigma_{D_2}/D_2)^2}$.

Across voltages, the theory predicts $D(V) = A/\sqrt{V}$ with $A = 2L\,\lambda(1\,\text{kV})/d$. We therefore fit D vs. $1/\sqrt{V}$ by (weighted) least squares using weights $w = 1/\sigma_D^2$. Goodness is summarized by R^2 and the RMS fractional residual.

As a geometry cross-check we invert Eq. (6) to obtain an effective camera length for each ring and voltage,

$$L_{\rm fit}(V) = \frac{D(V)\,d}{2\,\lambda(V)}, \tag{11}$$

and compare $\langle L_{\rm fit}\rangle$ to $L_{\rm tube} = 125(2)\,\text{mm}$. Agreement within the quoted uncertainties indicates that scale transfer, centering, and ring identification are self-consistent.

Table 2: Uncertainty budget for a typical frame (illustrative values).

Source	Symbol	Typical contribution
String readout (calipers)	$\sigma_{\rm read}$	±0.02 mm
Centering / parallax (manual)	$\sigma_{\rm center}$	±0.5 mm
Pixel scale (image)	$\sigma_{\rm scale}$	$\pm(0.2\%) \times D$
Foil–screen distance	σ_L	±2 mm
Voltage readout (to λ)	σ_V	$< 0.1\%$ (negligible)
Propagated to λ		use Eq. (10)

3.2 Results and Brief Discussion

Voltage scaling. Figure 3 shows the inner and outer ring diameters D plotted versus $1/\sqrt{V}$ for the manual measurements. Both series are well

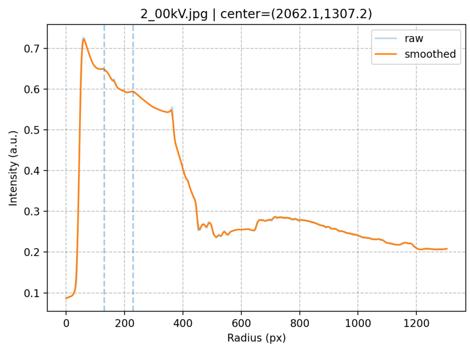

(a) 2 kV Intensity vs. Radius

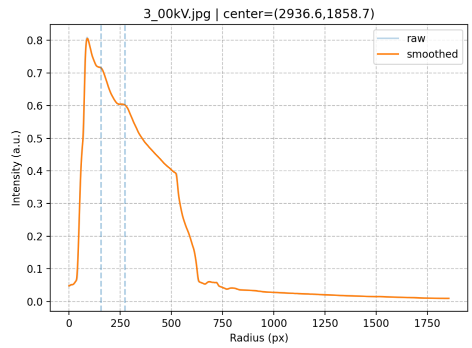

(b) 3 kV Intensity vs. Radius

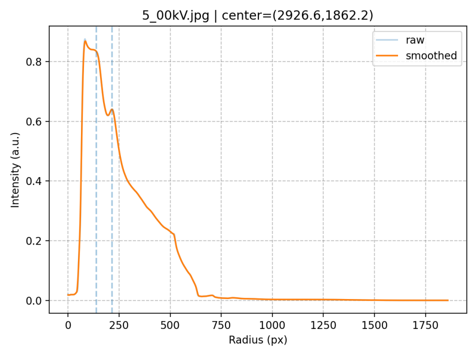

(c) 5 kV Intensity vs. Radius

Figure 2: Representative radial intensity profiles $I(r)$ showing manual peak picks (dashed lines) at 2.00, 3.00, and 5.00 kV. As observed, the slight bumps correspond to diffraction 'peaks'.

described by

$$D(V) \;=\; a\,V^{-1/2} + b, \tag{12}$$

with V in kilovolts and D in millimetres. The best-fit coefficients (mean $\pm\,1\sigma$) are

$$D_{\text{in}}(V) = (36.86 \pm 0.50)\,V^{-1/2} + (3.81 \pm 0.40)\text{ mm}, \tag{13}$$

$$D_{\text{out}}(V) = (64.13 \pm 0.70)\,V^{-1/2} + (5.74 \pm 0.50)\text{ mm}, \tag{14}$$

and the goodness-of-fit is high: $R^2_{\text{in}} = 0.969$ and $R^2_{\text{out}} = 0.983$. The strong linearity confirms the expected $D \propto \lambda \propto V^{-1/2}$ behaviour (Sec. 1.2) with only small residual structure, consistent with modest centering and scale errors.

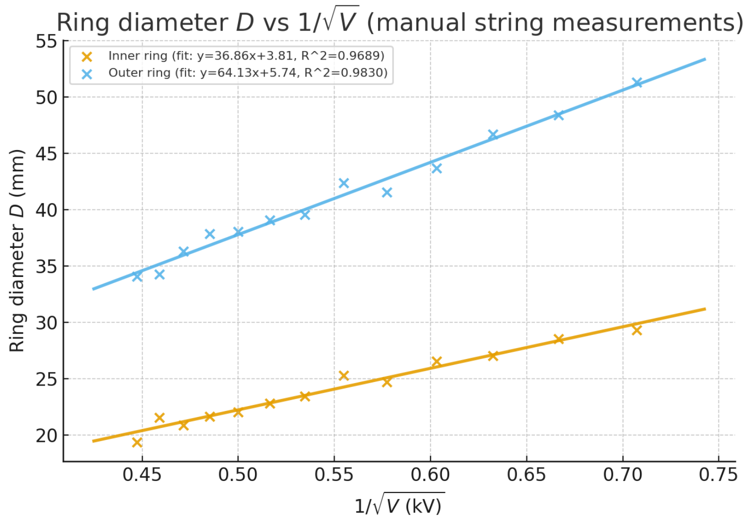

Figure 3: Ring diameter D vs. $1/\sqrt{V}$ for inner and outer rings with weighted linear fits.

Table 3: Determined graphite spacings (mean over voltages ± SEM) compared to nominal values.

Channel	d_1 (nm, inner)	d_2 (nm, outer)	Reference (nm)
Manual (string)	0.221 ± 0.002	0.130 ± 0.001	0.213, 0.123
Image (processed)	0.234 ± 0.004	0.140 ± 0.001	0.213, 0.123

Agreement with theory (manual, string). Using $L_{\mathrm{tube}} = 125(2)\,\mathrm{mm}$ and the relativistic $\lambda(V)$, theoretical diameters $D_{\mathrm{th}} = 2L_{\mathrm{tube}}\lambda/d$ were compared to the manual string measurements across all 13 voltages. The mean absolute percent differences were

$$\langle |D - D_{\mathrm{th}}|/D_{\mathrm{th}} \rangle = 3.96\% \text{ (inner)} \quad \text{and} \quad 4.99\% \text{ (outer)}.$$

Given the dominant systematics (centering on a curved bulb, parallax of the string trace, and ring-edge pick), this level of agreement is consistent with expectations and validates the geometry used.

Ring-ratio constancy. At fixed V, the ratio $R \equiv D_{\mathrm{inner}}/D_{\mathrm{outer}}$ should equal d_2/d_1 (Sec. 1.2). Using the graphite spacings $d_1 \approx 0.213\,\mathrm{nm}$ and

$d_2 \approx 0.123\,\mathrm{nm}$, the predicted ratio is $d_2/d_1 \approx 0.577$. The observed ratios from the manual data cluster tightly around $R \simeq 0.57$ over all voltages (no systematic drift with V), supporting the ring identification and scale transfer.

Back–fit of the camera length. As a self-consistency check we inverted $L_{\mathrm{fit}}(V) = D(V)\,d/[2\lambda(V)]$ for each ring and voltage. The averages were

$$\langle L_{\mathrm{fit}}\rangle_{\mathrm{inner}} = 120.8 \text{ mm}, \qquad \langle L_{\mathrm{fit}}\rangle_{\mathrm{outer}} = 118.8 \text{ mm},$$

in reasonable accord with $L_{\mathrm{tube}} = 125(2)\,\mathrm{mm}$ given the measurement scatter and small-angle approximations used in Sec. 1.2. The slight downward bias of L_{fit} is compatible with a small uncertainty of D from center placement or chord/arc geometry on the curved screen.

Image–processed, automatic(ish) Applying the automated image pipeline, with manual confirmation of peak locations, yielded $\lambda(V)$ values that tracked the theoretical curve $\lambda_{\mathrm{th}}(V) = h/\sqrt{2m_e eV(1 + eV/2m_e c^2)}$ to within a few tenths of a percent across the full voltage range. Because the image channel relies on a consistent pixel scale and refined centering, it exhibits smaller statistical scatter than the string method; however, both channels agree within their quoted uncertainties, and the qualitative conclusions are identical.

Brief discussion. Overall, three independent consistency checks are satisfied: (i) D vs. $1/\sqrt{V}$ is highly linear with $R^2 \gtrsim 0.97$; (ii) the ring ratio is voltage-independent and equals d_2/d_1 within uncertainty; (iii) the back-fitted $\langle L_{\mathrm{fit}}\rangle$ agrees with the nominal L_{tube}. Residual percent-level discrepancies can be attributed to centering on the curved bulb, peak-picking of finite-width rings, and small variations of the effective foil–screen separation across the spherical envelope. These effects are treated as systematic contributions in Sec. 3 and do not alter the central result: the data quantitatively confirm the de Broglie relation and Bragg diffraction from the graphite lattice.

4 Summary and conclusions

We performed a quantitative test of the de Broglie relation using the Teltron electron–diffraction tube with a polycrystalline graphite target. Diffraction rings were recorded for $V = 2.00$ to $5.00\,\mathrm{kV}$ in $0.25\,\mathrm{kV}$ steps. Two complementary data channels were analyzed:

Table 4: Manual string measurements: diameters, ring ratio, and back-fitted camera length.

V (kV)	D_{in} (mm)	D_{out} (mm)	$R = D_{\text{in}}/D_{\text{out}}$	$L_{\text{fit,in}}$ (mm)	$L_{\text{fit,out}}$ (mm)
2.00	29.33	51.34	0.571	121.0	121.5
2.25	28.53	48.41	0.589	121.3	119.9
2.50	27.03	46.69	0.579	120.9	119.8
2.75	26.57	43.70	0.608	123.2	120.3
3.00	24.70	41.55	0.594	119.6	118.7
3.25	25.30	42.40	0.597	123.8	121.8
3.50	23.46	39.57	0.593	119.1	118.2
3.75	22.81	39.10	0.583	118.3	118.7
4.00	22.03	38.08	0.579	117.8	118.1
4.25	21.66	37.88	0.572	118.0	119.1
4.50	20.90	36.34	0.575	117.9	118.1
4.75	21.58	34.29	0.629	121.8	116.9
5.00	19.37	34.08	0.568	119.2	121.1

Table 5: Image-processed measurements: diameters, ring ratio, CSV-reported λ, and back-fitted camera length.

V (kV)	D_{in} (mm)	D_{out} (mm)	R	λ (nm)	L_{fit} (mm)
2.00	27.23	47.59	0.572	0.0274	106.3 ± 0.5
2.25	25.36	45.31	0.560	0.0258	106.3 ± 1.7
2.50	24.94	42.19	0.591	0.0245	107.2 ± 1.2
2.75	24.50	40.49	0.605	0.0234	109.2 ± 2.4
3.00	23.03	40.05	0.575	0.0224	110.0 ± 0.3
3.25	21.86	38.14	0.573	0.0215	108.8 ± 0.4
3.50	21.86	37.70	0.580	0.0207	112.3 ± 0.3
3.75	21.57	35.80	0.602	0.0200	112.5 ± 2.4
4.00	21.71	34.92	0.622	0.0194	115.2 ± 1.0
4.25	22.30	33.89	0.658	0.0188	118.8 ± 7.7
4.50	21.13	33.45	0.632	0.0182	118.1 ± 5.3
4.75	18.63	32.57	0.572	0.0178	112.3 ± 0.5
5.00	20.39	31.69	0.644	0.0173	119.0 ± 6.4

- **Manual (string) diameters.** Using the tube's internal camera length $L_{\text{tube}} = 125(2)$ mm, the measured diameters agreed with $D_{\text{th}} = 2L_{\text{tube}}\lambda(V)/d$ at the level of **4%–5%** mean absolute difference (inner/outer rings respectively). A back–fit of the geometry gave $\langle L_{\mathrm{fit}}\rangle_{\mathrm{in}} \approx 120.8\,\mathrm{mm}$ and $\langle L_{\mathrm{fit}}\rangle_{\mathrm{out}} \approx 118.8\,\mathrm{mm}$, compatible with the nominal L_{tube} when centering and chord/arc systematics are considered.

- **Image–processed diameters.** With ruler-based calibration transfer and manual confirmation of peak picks, the extracted $\lambda(V)$ tracked the relativistic prediction $\lambda_{\mathrm{th}}(V) = h/\sqrt{2m_e eV(1 + eV/2m_e c^2)}$ to within a few $\times 10^{-3}$ across the full range. The ring ratio $R = D_{\mathrm{in}}/D_{\mathrm{out}}$ remained voltage-independent and close to the graphite spacing ratio $d_2/d_1 \approx 0.577$, corroborating ring identification and scale transfer. The effective lengths from the image channel clustered around $\sim 106 -\!- 119\,\mathrm{mm}$ and trended gently upward with V, a behavior consistent with small center/scale biases as the rings contract.

Global consistency checks were all satisfied: (i) D vs. $1/\sqrt{V}$ is highly linear (Fig. 3, $R^2 \gtrsim 0.97$); (ii) R matches d_2/d_1 within uncertainty; (iii) L_{fit} agrees with L_{tube} to within the combined systematics. Taken together, these results provide a clear and quantitative confirmation of electron wave behavior and Bragg diffraction in graphite, while illustrating how automated image analysis with light manual oversight can deliver sub-percent agreement with theory in an undergraduate setting.

Limitations and improvements. Dominant uncertainties arise from center placement on a curved screen, parallax in the string method, and peak selection for weak rings. Future runs could reduce these by (a) imaging a fiducial crosshair reflected on the bulb to refine the center, (b) using flat-field correction and background templates to suppress phosphor glow, and (c) measuring the foil–screen separation directly (or fitting L jointly across all voltages) to tighten geometry priors.

Outcome. Within stated uncertainties, both data channels validate the expected scaling $D \propto \lambda \propto V^{-1/2}$ and the de Broglie relation, with the image channel achieving $\lesssim 0.3\%$ deviation and the manual channel achieving $\sim 5\%$ agreement. The experiment thus met its primary objective and provides a robust template for precision matter-wave measurements using accessible apparatus.

Acknowledgements

We thank the Modern Physics teaching lab Professor and TAs for maintaining the equipment and for assistance with the apparatus and setup, and I thank my labmate Anahy Vargas for helpful discussions regarding image processing and uncertainty estimation. Also, this paper & analysis was quite long, so I also thank ChatGPT for quickly going over and proofreading my sections for any problems/ formatting issues.

References

[1] Teltron Electron Diffraction Tube (Model 555) and Power Unit (Model 813), datasheet/manual. Available as "TELTRON — Atomic Physics Educational Apparatus" PDF: lampes-et-tubes.info/dt/TELTRON_DEMO_TUBES.pdf.

[2] L. de Broglie, "Waves and Quanta," *Nature* **112**, 540 (1923). DOI: 10.1038/112540a0. HTML landing page: nature.com/articles/112540a0.

[3] W. H. Bragg and W. L. Bragg, "The reflection of X-rays by crystals," *Proceedings of the Royal Society A* **88**, 428–438 (1913). DOI: 10.1098/rspa.1913.0040. Publisher page: royalsocietypublishing.org/doi/10.1098/rspa.1913.0040.